THE INFLUENCE OF TEMPERATURE ON THE STRAIN-RATE DEPENDANT MATERIAL BEHAVIOUR OF CFRP UNDER HIGH-DYNAMIC LOADING

W. A. Hufenbach[1], A. Langkamp[1], R. Bochynek[2]*
[1] Institute of Lightweight Engineering and Polymer Technology, TU Dresden, Holbeinstr. 3, 01307 Dresden, Germany
[2] Leichtbau-Zentrum Sachsen GmbH, Marschnerstr. 39, 01307 Dresden, Germany
* Corresponding author (bochynek@lzs-dd.de)

Keywords: *carbon fibre-reinforced composites, strain-rate dependence, temperature loading, high-dynamic loading*

1 General introduction

Especially the material class of carbon fibre-reinforced composites combines low weight and high strength with good impact behaviour, what makes them quite attractive to applications in the aerospace industry. Nevertheless, the lack of trusted data and knowledge of damage and failure mechanisms under high-dynamic loading such as impact often leads to highly conservative design of structural components.

Due to very complex failure mechanisms in textile-reinforced composites [1-3] an adequate prediction of material behaviour after impact is still difficult, even if the strain-rate dependence of material data determined in coupon testing of unidirectional-reinforced composites is well known [4-5]. Since the specific textile architecture influences highly the mechanical behaviour of carbon fibre-reinforced composites, a very large number of additional tests are necessary to determine elastic and strength as well as damage and strain rate parameters for an adequate numerical modelling. The strain rate dependent in-plane and through thickness behaviour of textile-reinforced composites based on hybrid glass/polypropylene yarn has been investigated in detail experimentally and numerically [6-8].

Due to the large variety of different textile reinforcements and for reduction of experimental effort as well as costs, simple tests are required to determine the ability of different textile configurations for specific multi-axial load cases. A comprehensive comparative study regarding different textile reinforcement architectures is presented in [9].

Especially in aerospace applications, impact events with high loading velocities are common multi-axial loading cases. By the detailed consideration of such an impact event, two dominating basic load cases are identified. Global bending and local through thickness shearing caused by the high-dynamic loading of an impactor are observed.

Furthermore temperature loadings play an important role in aerospace applications. It is well known that material behaviour is strongly dependant on the environmental temperature and has to be considered. Common temperature levels in aerospace applications are in a range of -55 °C and 200 °C

Adapted testing rigs have to be designed to investigate the global bending and through thickness shearing behaviour. Experimental investigations of these basic load cases are performed with a bending testing rig (see Fig 2) at a servo-hydraulic high velocity test system. The application of a combined bending and through thickness shearing loading is applied by a reduced distance of the supporting bars of the testing rig. Contrary to conventional 3-point-bending test a high percentage of shear loading is introduced into the specimen.

For conventional quantitative analysis of the experiments by force-displacement-curves, the force measurement system is located in the impactor to reduce the influence of oscillation of the testing rig while loading. For qualitative analysis of damage and failure behaviour of different textile-reinforced composites, a high speed camera system with a maximum frame rate of up to 200,000 images per second was used.

Within the scope of this work, the damage and failure behaviour after bending loading of the conventional non-crimp fabric is compared at different temperature levels from -50 °C to 200 °C. The quantitative and qualitative analysis shows varying strain-rate dependence at different temperature levels.

2 Experimental concept

2.1 Material configurations

The textile architecture of the carbon fibre-reinforced composites plays an important role on the strain rate dependant material behavior at combined bending and shearing loading. Within the scope of this work, the damage and failure behavior of conventional non-crimp fabric is compared with them of a woven fabric. In Fig. 1 CT-scans of each textile configuration are shown.

Non-crimp fabrics are characterized by the straightened orientation of the roving. Due to the non-existence of crossing points in a single layer, mechanical properties such as stiffness and strength show the best possible performance. The poor compound between the rovings of a layer results in an insufficient drapability.

Woven fabrics are characterized by orthogonally crossed rovings. The large variety of different types of woven fabrics results in a wide range of mechanical and manufacturing properties. Compared to non-crimp fabrics, woven fabrics show a much better drapability. The ondulation of the rovings causes decreasing mechanical properties. In this work a plain weave is investigated.

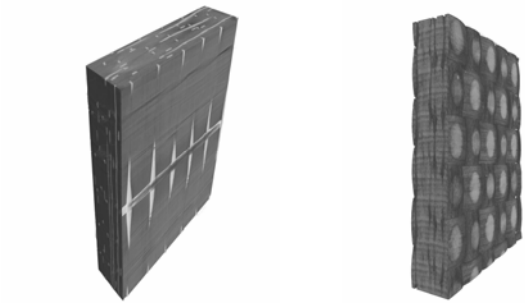

Fig. 1. CT-scans of textile configurations: non-crimp fabric (left) and woven fabric (right)

The different textile configurations consist of carbon fibre system Tenax HTS40 from TohoTenax. For consolidation the epoxy matrix system HexFlow® RTM 6 from Hexcel is used, which is specially developed for aerospace applications. The specimen panels with a thickness of 8 mm have been manufactured by resin transfer moulding (RTM) [10]. Specimen preparation has been performed by waterjet cutting.

2.2 Testing at different temperature domains

For investigation of the temperature dependant material behavior at different strain rate levels a novel testing chamber has been designed, which is shown in Fig. 2. High-dynamic tests at the servo hydraulic high velocity test system Instron VHS 160/20 require manifold constructive details [11]. To ensure a constant testing temperature a double-walled metal sheet design has been chosen. For minimising the thermal loss during testing, a specific chamotte isolation layer has been applied between both metal sheet layers. For the isolation of connection areas a non-shrink adhesive system on a silicone basis has been used, which additionally compensates thermal shrinkage of the whole chamber when applying different temperature levels.

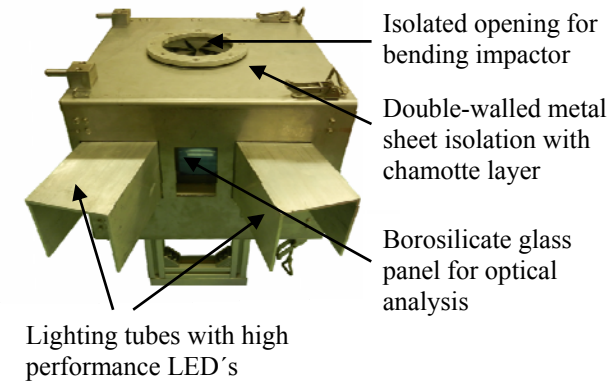

Fig. 2. Testing chamber for high-dynamic testing at temperature levels from -55 °C to 200 °C

Especially in the field of high-dynamic testing, the usage of optical measurement methods is essential for analyzing the damage behavior of the tested materials. Enabling the usage of high speed camera

systems for the optical recording of experiments at lower or higher temperature levels represents a big challenge to the design process of the testing chamber. Due to the high requirements a high temperature-stable borosilicate glass with a very low thermal expansion coefficient has been chosen. Additionally, the surface of the glass panel is of a very high quality due to a specific patented manufacturing process, which ensures the recording of non-reflective pictures with high speed camera systems.
The lighting system of the testing chamber should be placed outside of the inner space to ensure a constant temperature inside the testing chamber. To minimize the influence on the recordings of the high speed camera system, the lighting tubes are isolated from the optical measurement tube. For lighting of the inner space high performance light-emitting diodes has been placed in the lighting tubes.
Furthermore at the inner space of the testing chamber a special non-reflecting coating is applied to reduce the influence of reflections on the optical measurement with the high speed camera.

2.3 Testing setup

A servo hydraulic high velocity test system Instron VHS 160/20 has been utilised for the experiments. This rig enables tests at high deformation speeds of up to 20 m/s with a maximum force of 160 kN. Especially at high loading velocities, oscillations caused by the testing rig interact with the original loading measurement system located below the testing devices and may cause hardly analysable measurement data [12]. Therefore, a new force measurement system has been developed, which is located inside the impactor. Forces are measured directly by strain gauges at the contact area between impactor and specimen, whereby the influence of oscillation on the force measurement is decreased significantly. Beside conventional force and displacement measurement the high speed camera system Phantom v7.2 with a maximum frame rate of up to 200,000 images per second was used for damage and failure analysis of the combined bending and shearing tests [12].
Investigations of the combined bending and shearing behaviour have been performed with a 3-point bending device (see Fig. 3). Load is applied with a straight fin with diameter of 5 mm and a length of 20 mm. Both supports of the testing device have a distance of 64 mm and a radius of 2 mm. The rectangular bending specimens have a length of 80 mm, a width of 20 mm and a thickness of 8 mm.
A combined bending and shearing loading is achieved by a reduction of the distance of the supporting bars compared to conventional 3-point-bending according to DIN EN ISO 2764 [12]. The reduction of the supporting bar distance to 64 mm results in a shearing loading percentage of 80 % and a bending loading percentage of about 20 %.
The rig is located inside the testing chamber. To ensure correct temperature level, a second specimen with an integrated thermocouple is placed near the tested specimen.

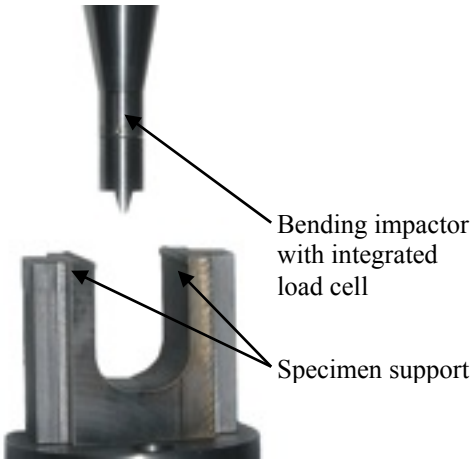

Fig. 3. Testing rig with rectangular specimen and diagram of distribution of bending and shearing loading of the investigated material configuration

2.4 Testing parameters

Material tests at room temperature have been performed at five nominal loading velocities (0.0001 m/s, 0.001 m/s, 0.01 m/s, 0.1 m/s and 1 m/s) for each textile configuration (see Tab 1). Tests at high and low temperature levels have been performed at three nominal loading velocities (0.0001 m/s, 0.01 m/s, and 1 m/s). With four to five repetitions per loading velocity and temperature level a series of 100 experiments has been performed for each material configuration, which results in a total number of 200 experiments.

In these testing configurations conventional in-plane strain measurement with strain gauges has not been performed. Nominal strain rates of the combined bending and shearing tests have been calculated according DIN EN 2764 [13] with the following equation:

$$\dot{\varepsilon} = \frac{6 \cdot h \cdot v}{L^2} \tag{1}$$

where v is the loading velocity, L is the distance between both supports of the testing device and h is thickness of the specimens. The occurring strain rates for each textile configuration are analysed with equation (1) and presented in Tab. 1.

Nominal temperature level	Exp. determined strain rates [s^{-1}]
-50 °C	$3 \cdot 10^{-3}$; $3 \cdot 10^{-1}$; $2.5 \cdot 10^{1}$
-20 °C	$3 \cdot 10^{-3}$; $3 \cdot 10^{-1}$; $2.5 \cdot 10^{1}$
23 °C	$3 \cdot 10^{-3}$; $3 \cdot 10^{-2}$; $3 \cdot 10^{-1}$; $3 \cdot 10^{0}$; $2.5 \cdot 10^{1}$
60 °C	$3 \cdot 10^{-3}$; $3 \cdot 10^{-1}$; $2.6 \cdot 10^{1}$
120 °C	$3 \cdot 10^{-3}$; $3 \cdot 10^{-1}$; $2.6 \cdot 10^{1}$
160 °C	$3 \cdot 10^{-3}$; $3 \cdot 10^{-1}$; $2.6 \cdot 10^{1}$
200 °C	$3 \cdot 10^{-3}$; $3 \cdot 10^{-1}$; $2.6 \cdot 10^{1}$

Tab. 1. Temperature and strain rate levels for both textile configurations (non-crimp fabric and woven fabric)

3 Experimental results and material parameters

3.1 Determination of material properties

Based on the discussed testing setup four to five force-displacement curves have been measured for each material configuration within each strain rate and temperature domain.
For further analysis characteristic stiffness, strength and energy based material parameters are determined for all testing and material configurations. These are the bending stiffness E_f, the maximum impact force F_M and the characteristic impact energy W_C. The bending stiffness is determined by linearization of bending stress-bending strain curve within a range of 0.05 % and 0.25 bending strain. Maximum impact force is defined by the maximum of the force-displacement curve until significant decrease which is equivalent to failure of the specimen. Characteristic impact energy is defined by the area below the force-displacement curve until specimen failure which is defined by 10 % of the maximum impact force. All material parameters are arithmetically averaged over the number of tests.

3.2 Strain rate dependence

For exact quantitative comparison of the considered testing configurations, the strain rate dependence at each temperature level is focused on the experimentally determined stiffness (see equation 2), strength (see equation 3) and energy (see equation 4) parameters and was found to be accurately described within the experimental limits by the Johnson-Cook [14] based equations:

$$E_f\left(\dot{\varepsilon}\right) = E_f^{ref}\left[1 + A^E \ln\left(\frac{\dot{\varepsilon}}{\dot{\varepsilon}^{ref}}\right)\right] \tag{2}$$

$$F_M\left(\dot{\varepsilon}\right) = F_M^{ref}\left[1 + A^F \ln\left(\frac{\dot{\varepsilon}}{\dot{\varepsilon}^{ref}}\right)\right] \tag{3}$$

$$W_C\left(\dot{\varepsilon}\right) = W_C^{ref}\left[1 + A^W \ln\left(\frac{\dot{\varepsilon}}{\dot{\varepsilon}^{ref}}\right)\right] \tag{4}$$

In these equations E_f, F_M and W_C represent the bending stiffness, the maximum impact force and the characteristic impact energy of each material configuration at the current strain rate ε. The reference values E_f^{ref}, F_M^{ref}, and W_C^{ref} at a reference strain rate ε^{ref} and the material constants A^E, A^F and A^W describe the strain rate dependant behaviour of stiffness, strength and energy parameters. It has to be emphasized, that these equations describe the material behaviour at least within the range of the experimentally investigated strain rate domains. A prediction of parameters outside of this range may results in unreasonable values [12].
In Fig. 4 to Fig. 9 the strain rate dependence of the characteristic stiffness, strength and energy

parameters is presented, whereby two kinds of diagram types have been chosen. The two-dimensional diagrams show the strain rate dependence of the characteristic parameter at each temperature level. For a better understanding of the complex correlations between characteristic stiffness, strength and energy parameters and strain rate and temperature domains, the experimental results are displaced in a three-dimensional diagram as well.

The experimentally determined values can be described accurately by the model parameters. With the help of these model parameters, it is possible to analysis the strain rate dependant bending behaviour of the investigated material configurations and to draw important conclusions on the temperature and strain rate dependant material behaviour of different textile architecture of CFRP.

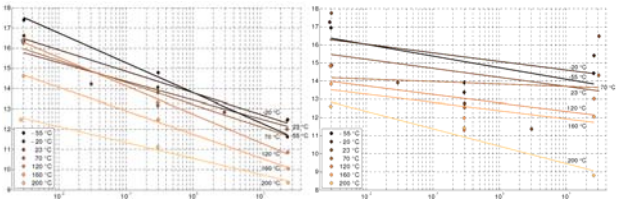

Fig. 4. Bending stiffness vs. strain rate curves at different temperature domains of non-crimp fabric (left) and woven fabric (right)

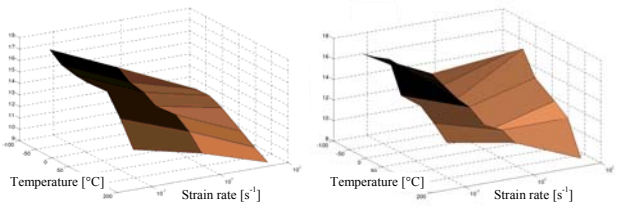

Fig. 5. Bending stiffness vs. strain rate and temperature of non-crimp fabric (left) and woven fabric (right)

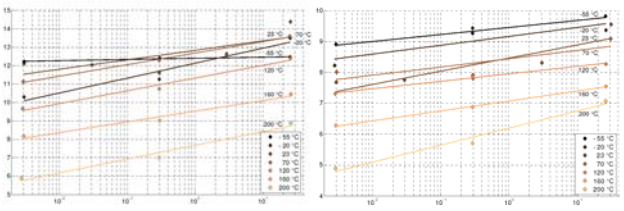

Fig. 6. Maximum force vs. strain rate curves at different temperature domains of non-crimp fabric (left) and woven fabric (right)

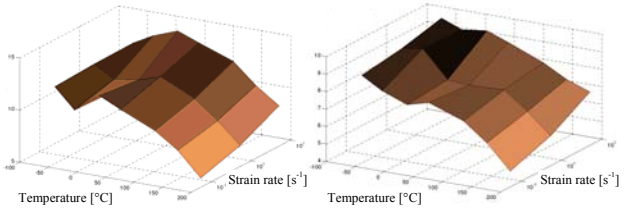

Fig. 7. Maximum force vs. strain rate and temperature of non-crimp fabric (left) and woven fabric (right)

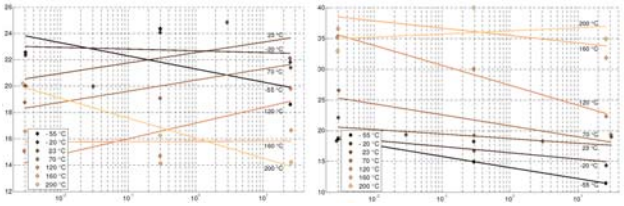

Fig. 8. Characteristic energy vs. strain rate curves at different temperature domains of non-crimp fabric (left) and woven fabric (right)

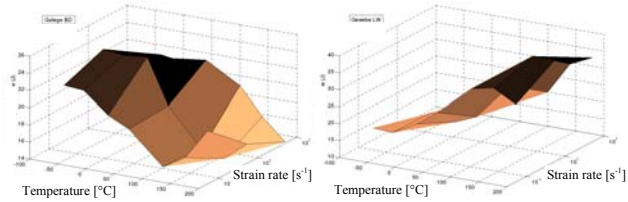

Fig. 9. Characteristic energy vs. strain rate and temperature of non-crimp fabric (left) and woven fabric (right)

The following conclusions can be drawn:

- Both material configurations show a decreasing bending stiffness with increasing strain rate at all temperature levels. Here, the amount of decreasing is slightly lower for woven fabric specimens.
- Both material configurations show a decreasing bending stiffness with increasing temperature level.
- Both material configurations show an increasing maximum force with increasing strain rate.
- Both material configurations show an increasing maximum force with decreasing temperature level.
- Non-crimp fabric specimens show a decreasing characteristic energy at temperature levels of -55 °C, -20 °C and 200 °C and an increasing characteristic energy at temperature levels of

23 °C, 70 °C, 120 °C and 160 °C with increasing strain rate.

- Woven fabric specimen show a decreasing characteristic energy at all temperature levels with increasing strain rate.

3.3 Damage and failure analysis

All tests have been recorded with the high speed camera system Phantom v7.2 to perform a detailed damage and failure analysis. In Fig. 10 to Fig. 13 the damage evolution of non-crimp fabric and woven fabric specimens at selected temperature domains and a medium strain rate of $3 \cdot 10^{-1}$ s^{-1} is shown. Here temperature levels of -55 °C (see Fig. 10), 23 °C (see Fig. 11), 120 °C (see Fig. 12) and 200 °C (see Fig. 13) are considered, whereby high speed recordings are dedicated to specific points on the force-displacement curves.

The non-crimp fabric specimens show a very early compared to the other material configuration beginning of delamination between the single layers of the specimens. After catastrophic failure nearly all layers are separated and delaminated. The woven fabric shows a similar behaviour but in a weakened form.

Furthermore, at low temperature levels more brittle failure behaviour is observed. With increasing testing temperature level it changes to a more smooth damage and failure behaviour. This behaviour is more pronounced for woven fabric specimens. At temperature levels from -55 °C to room temperature a catastrophic failure can be occurred at the end of the loading, whereas at higher temperature levels the specimens show high deformation without catastrophic failure.

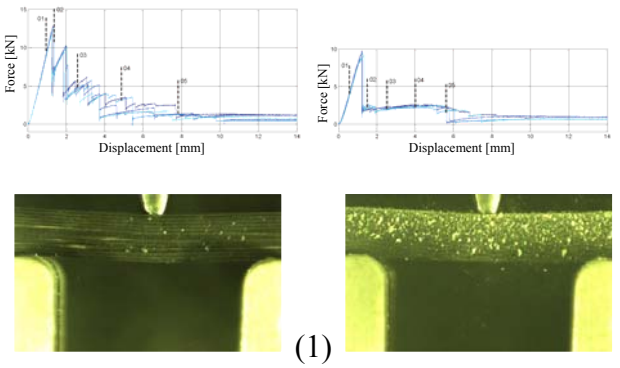

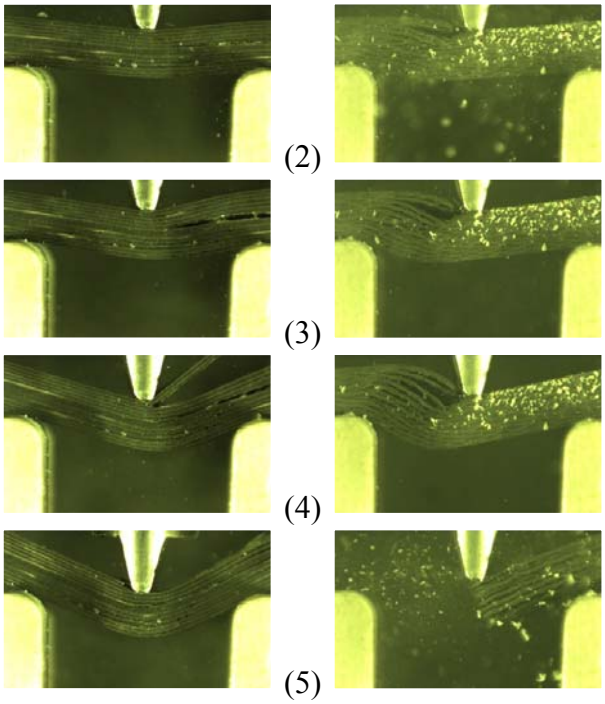

Fig. 10. Damage and failure evolution at a temperature level of -55 °C of non-crimp fabric (left) and woven fabric (right)

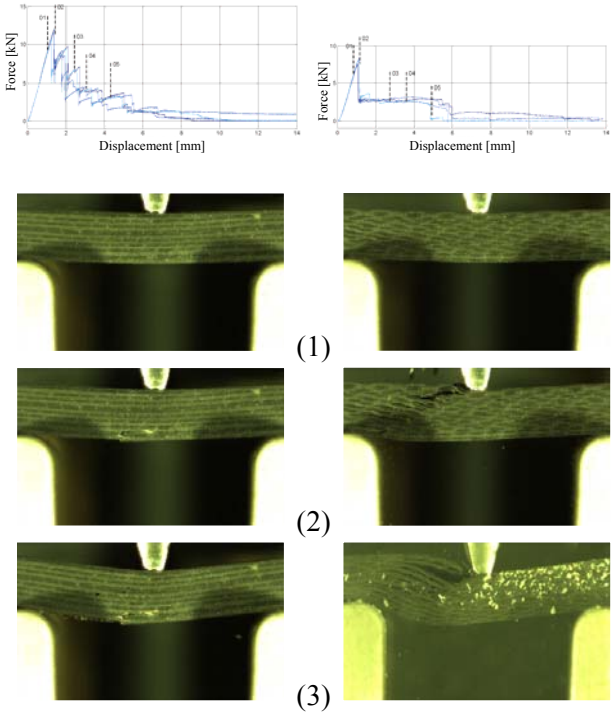

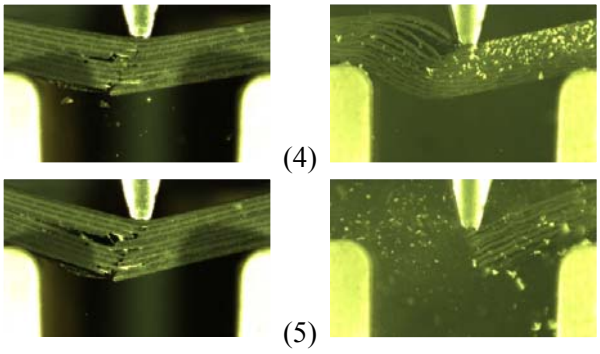

Fig. 11. Damage and failure evolution at room temperature of non-crimp fabric (left) and woven fabric (right)

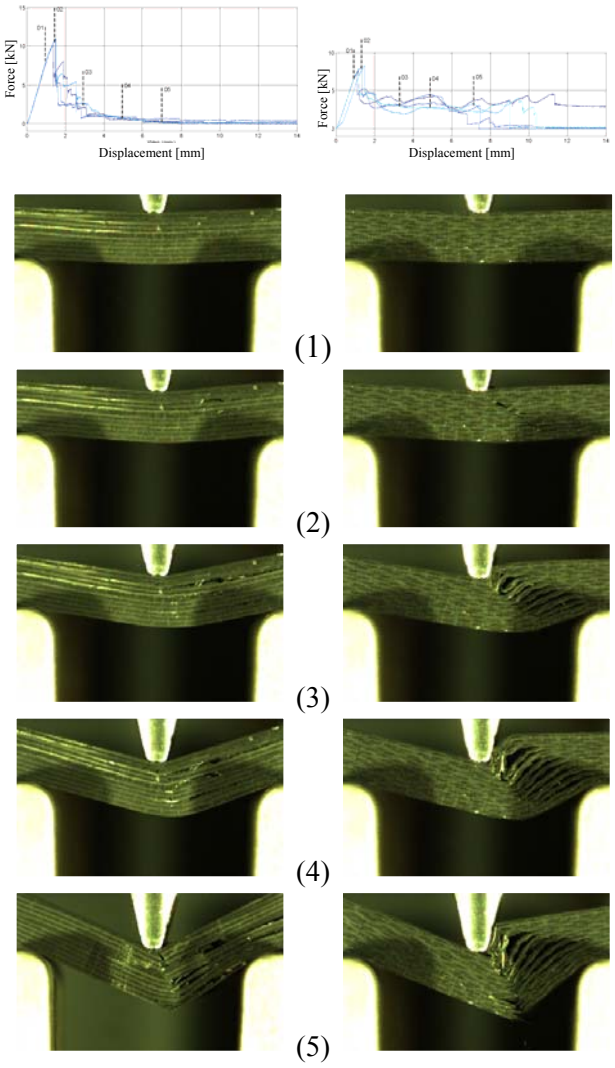

Fig. 12. Damage and failure evolution at a temperature level of 120 °C of non-crimp fabric (left) and woven fabric (right)

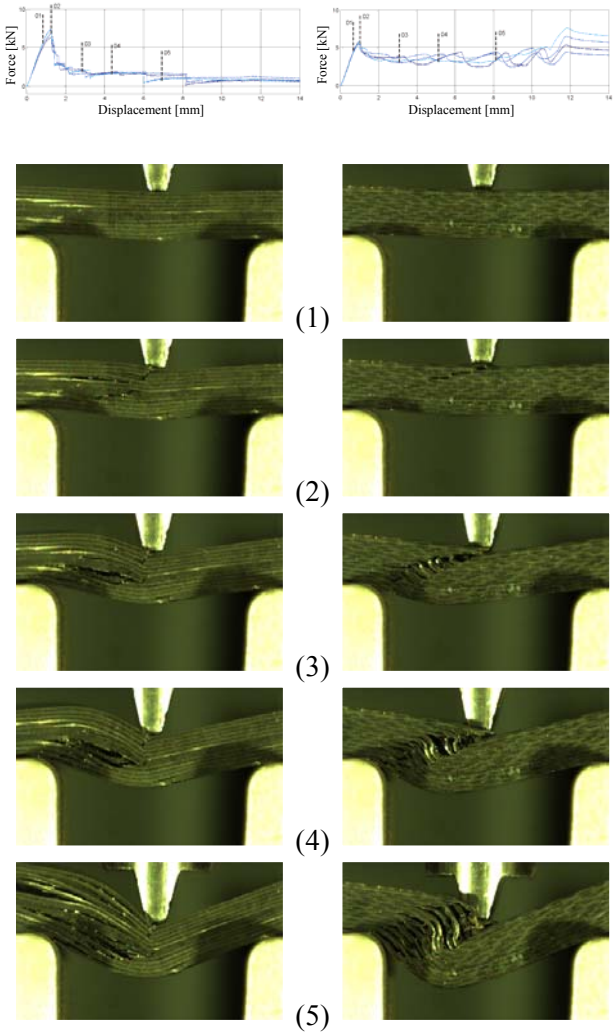

Fig. 13. Damage and failure evolution at a temperature level of 200 °C of non-crimp fabric (left) and woven fabric (right)

4 Summary and conclusions

Within the scope of this work the strain rate dependant material behaviour of carbon fibre-, textile reinforced composites at different temperature domains has been investigated. High-dynamic 3-point-bending tests with resulting strain rates from $3 \cdot 10^{-3}$ s^{-1} to $2.5 \cdot 10^{1}$ s^{-1} have been performed at common aerospace temperature levels from -55 °C to 200 °C. Two material configurations with different textile architectures, a non-crimp fabric and a woven fabric have been considered.

A novel testing chamber has been designed to investigate the material behaviour at different strain rate and temperature levels. With this testing

chamber the realisation of high-dynamic tests using the servo hydraulic high velocity test system Instron VHS 160/20 at low and elevated temperature domains is possible. Furthermore, an optical analysis of the damage and failure behaviour can be performed as well as optical strain measurement methods can be applied due to the usage of a non-reflective and temperature-resistant Borosilicate glass panel.

Testing results have been analysed with respect to characteristic stiffness, strength and energy parameters and Johnson-Cook based model parameters have been determined to describe, compare and evaluate the temperature and strain rate dependant material behaviour of the considered material configurations.

Additionally, a phenomenologically based analysis of the damage and failure with a high-speed camera system has been performed. From these results important conclusions on the ability for applications in high dynamic loaded impact structures can be drawn.

Acknowledgments

Experimental investigations and development of testing rigs have been performed within the testing laboratory of the Leichtbau-Zentrum Sachsen GmbH. The authors wish to express their thanks for the support.

References

[1] R. Böhm, M. Gude, W. A. Hufenbach: "A phenomenologically based damage model for 2D and 3D-textile composites with non-crimp reinforcement". *Materials and Design*, Vol. 32, pp. 2532-2544, 2011.

[2] R. Gerlach, C. R. Siviour, J. Wiegand, N. Petrinic: "In-plane and through-thickness properties, failure modes, damage and delamination in 3D woven carbon fibre composites subjected to impact loading". *Composites Science and Technology*, Vol. 72, pp. 397–411, 2012.

[3] R. Böhm, M. Gude, W. A. Hufenbach: "A phenomenologically based damage model for textile composites with crimped reinforcement". *Composites Science and Technology*, Vol. 70, pp. 81–7, 2010.

[4] W. Wang, G. Makarov, R. A. Shenoi: "An analytical model for assessing strain rate sensitivity of unidirectional composite laminates". *Composite Structures,* Vol. 69, pp. 45–54, 2005.

[5] R. L. Sierakowsky: "Strain rate effects in composites". *Applied Mechanics Reviews*, Vol. 50, pp. 741–761, 1997.

[6] W. A. Hufenbach, A. Langkamp, A. Hornig, M. Zscheyge, R. Bochynek: "Analysing and modelling the 3D shear damage behaviour of hybrid yarn textile-reinforced thermoplastic composites". *Composite Structures,* Vol. 94, pp. 358–368, 2011.

[7] W. A. Hufenbach, A. Hornig, B. Zhou, A. Langkamp, M. Gude: "Determination of strain rate dependent through-thickness tensile properties of textile reinforced thermoplastic composites using L-shaped beam specimens". *Composite Science and Technology*, Vol. 71, pp. 1110-1116, 2011.

[8] W. A. Hufenbach, M. Gude, C. Ebert, M. Zscheyge, A. Hornig: "Strain rate dependent low velocity impact response of layerwise 3D-reinforced composite structures". *International Journal of Impact Engineering,* Vol. 38, pp. 358–368, 2011.

[9] W. A. Hufenbach, R. Böhm, M. Thieme, A. Winkler, E. Mäder, J. Rausch, M. Schade: "Polypropylene/glass fibre 3D-textile reinforced composites for automotive applications". *Materials and Design,* Vol. 32, pp. 121–131, 2011.

[10] W. A. Hufenbach (Ed.): *"Textile Verbundbauweisen und Fertigungstechnologien für Leichtbaustrukturen des Maschinen- und Fahrzeugbaus"*. Progress media-Verlag, Dresden, 2007.

[11] M. Graupner: *"Experimental investigations on the temperature behaviour of carbon-fibre reinforced composites at complex loading cases".* Diploma thesis, TU Dresden, 2013.

[12] W. A. Hufenbach, O. Renner, R. Bochynek, A. Hornig: "The influence of textile architecture on the strain-rate dependant material behaviour of carbon fibre-reinforced composites under bending loading". *ECCM15, Venice, Italy,* 2012.

[13] DIN EN 2746: *„Luft- und Raumfahrt - Glasfaserverstärkte Kunststoffe - Biegeversuch – Dreipunktverfahren"*. Beuth Verlag, Berlin, 1998.

[14] G. R. Johnson, W. H. Cook "Fracture characteristics of three metals subjected to various strains, strain rates, temperatures and pressures". *Engineering Fracture Mechanics,* Vol. 21 No. 1, pp. 31-48, 1985.